

FRACTAL ROUGHNESS REPRESENTATION IN A STOCHASTIC ONE-DIMENSIONAL TURBULENCE MODELING APPROACH

Juan A. Medina Méndez
Numerische Strömungs-
und Gasdynamik
BTU Cottbus-Senftenberg
Cottbus, Germany
medinjua@b-tu.de

Marten Klein
Numerische Strömungs-
und Gasdynamik
BTU Cottbus-Senftenberg
Cottbus, Germany
marten.klein@b-tu.de

Heiko Schmidt
Numerische Strömungs-
und Gasdynamik
BTU Cottbus-Senftenberg
Cottbus, Germany
heiko.schmidt@b-tu.de

ABSTRACT

The present study aims to capture drag effects resulting from turbulent flows in wall-bounded configurations with homogeneous roughness. The focus is on the formulation of a reduced model which allows turbulent boundary-layer-type flow simulations without the usual computational overhead associated to 3-D numerical simulations requiring faithful surface topology representation and associated boundary conditions. The framework of the model is derived from volume-averaging theory (VAT). On one hand, a Darcy-like 1-D model enables a reduced dynamical representation of roughness effects for the wall-normal coordinate. The effect of the turbulent flow, which is not usually part of Darcy-like models, is considered by incorporating the effect of the hydrodynamic dispersion tensor using a map-based stochastic approach. The latter is known as One-Dimensional Turbulence (ODT) in standalone applications. The comprehensive modeling framework allows then the full-scale resolution of wall-normal transport processes in a relatively inexpensive 1-D computational domain. We first test and compare the performance of the ODT standalone application using a previously published ad-hoc parametric forcing approach (PFA) for Direct Numerical Simulations (DNS) of turbulent flows over homogeneous roughness. These results are compared to those of simulations using the suggested VAT-derived model for the homogeneous roughness. To that extent, we show that simulated roughness-induced drag and wall-normal stress contributions are comparable to available direct numerical simulation (DNS) data. In comparison to the ad-hoc PFA, the new suggested VAT-derived model allows more physical insights regarding the effects of the form of the homogeneous roughness (statistical moments) on the stress contributions.

CONTEXT AND SIGNIFICANCE

Roughness and turbulence may very well be two of the most naturally occurring phenomena. Most industrially relevant flows are turbulent, and most engineering surfaces are also rough. Although formally a field of aerodynamics and fluid mechanics, the interactions between rough surfaces and turbulent flows are studied in a wide field of disciplines. The atmospheric boundary layer over canopies or buildings is a related formal topic in atmospheric sciences as in Cooke *et al.* (2024), civil and structural engineering as in Toja-Silva *et al.* (2018), and similar. Corrosion can also be considered as a closely related formal discipline for more technical applica-

tions, see Thorat *et al.* (2024) for applications. Recent discussions on the importance of understanding roughness and full-scale drag predictions situate drag uncertainty estimates on a range of 10 – 30%. In the context of the naval or aerospace industry, this amounts to a very significant part of the costs, or conversely, of the potential profits, see Chung *et al.* (2021) for details.

In an age of ample computational development, Direct Numerical Simulations (DNS) are the method of choice for accurate prediction of drag generated over rough surfaces. Attempts to fully resolve surface topology in DNS are an active research field, and techniques such as conformal mappings, immersed boundary methods or discrete element methods are frequently used, see e.g., Busse *et al.* (2015). Generalization of DNS studies done in this way is extremely difficult. On one hand, DNS with accurate topology representation are computationally very expensive, and as such, there are not that many published DNS studies. On the other hand, it is not an easy task to decide on the relevant length scales of the roughness which aid towards generalization and universality. To that extent, understanding roughness-turbulence interactions necessarily involves first a discussion on roughness characterization. Consensus seem to revolve around using both the statistical distribution of roughness peak heights, i.e., the probability density function (PDF) of roughness heights, as well as the spatial correlation of the roughness, which could be represented by a horizontal-wavenumber power spectrum, see Pérez-Ràfols & Almqvist (2019). These studies motivate our choice for roughness characterization in the modeling approach.

STANDALONE APPLICATION OF ODT USING AD-HOC DRAG PARAMETRIC FORCING

As a first part of this study we focus on the standalone application of the One-Dimensional Turbulence (ODT) model with an ad-hoc parametric forcing approach (PFA) for roughness drag. The PFA introduces the effect of the roughness by means of a source term in the Navier-Stokes momentum equation, see Busse & Sandham (2012). The form of the source term, however, was not originally related to the surface geometry of the roughness. One important step towards a more geometry-related form of the roughness term in the PFA is found in the approach followed by Forooghi *et al.* (2018), who introduces a source term $f_{F,i}$ in the form of a Darcy-

Forchheimer model,

$$f_{F,i}(y) = -A(y)u_i - B(y)u_i|u_i| \quad (1)$$

No summation is implied over repeated indices for the previous equation. The velocity field is noted as u_i for $i \in \{1, 2, 3\}$. Also, $A(y)$ and $B(y)$ are wall-normal dependent coefficients which are formulated on the basis of the kinematic viscosity ν , the wall-normal porosity profile $\varepsilon(y)$, the interface area per unit total volume $s(y)$, and the projected frontal surface area per unit total volume $s_f(y)$. The latter profiles can all be obtained for a given rough surface. In summary,

$$A(y) = k_K \frac{\nu s^2(y)}{\varepsilon(y)}, \quad B(y) = c_D \frac{s_f(y)}{2} \quad (2)$$

Although Forooghi *et al.* (2018) is able to formulate a model which replaces the arbitrary form of the forcing function from Busse & Sandham (2012) by a more physical formulation as in Eq. (1), the model falls short when two arbitrary constant coefficients are introduced in Eq. (2). These are k_K and c_D , which can be interpreted as a Carman-Kozeny constant and a type of drag coefficient, respectively. Needless to say, there is no formal derivation from first principles that can be made for these coefficients which somehow relates them to the homogeneous surface geometry. To that extent, Forooghi *et al.* (2018) performs DNS of open channel turbulent flows in order to determine k_K and c_D for some selected roughness geometries at specific Reynolds numbers.

We intend to test the effect of the coefficients found for the PFA by Forooghi *et al.* (2018) in the reduced order One-Dimensional Turbulence (ODT) model. ODT is a map-based stochastic turbulence model, see Kerstein (1999). Its best application is on turbulent flows which exhibit statistics dominated by velocity gradients in one direction. This is usually the case for most boundary-layer flows. Following previous related applications of ODT for wall-bounded flows, e.g., in Lignell *et al.* (2013); Klein *et al.* (2022), we utilize a temporal ODT formulation which evolves scalar velocity component profiles on a wall-normal domain parallel to the planar coordinate y . The governing equations for the velocity components u_i , where u_1 is the streamwise-directed and u_2 the wall-normal-directed component, can be written as

$$\frac{\partial u_i}{\partial t} + \mathcal{M}(u_i) = -\frac{1}{\rho} \frac{d\bar{p}}{dx} \delta_{i1} + \nu \frac{\partial^2 u_i}{\partial y^2} + f_{F,i} \neq 2 \quad (3)$$

Here, ρ and ν are the density and kinematic viscosity of the fluid, assumed constant, respectively. Note the dynamic viscosity $\mu = \rho\nu$. Likewise, $-d\bar{p}/dx$ is a constant pressure-gradient forcing the flow, which corresponds to the time-averaged pressure gradient balancing the wall-shear stress in the wall-bounded configuration. Also, δ_{i1} is 1 for $i = 1$ and zero otherwise. No forcing is applied on the u_2 velocity component. Regarding the ODT model, $\mathcal{M}(u_i)$ is the model-represented turbulent advection and pressure-scrambling effect. Eq.(3) is integrated numerically in time as in a 1-D DNS, yet as seen, this numerical integration procedure only observes the mean pressure gradient, the drag forcing, the viscous term, and the advection of u_i by the mean velocity \bar{u}_2 in the wall-normal direction; the latter is zero from usual boundary-layer assumptions on fully-developed flow and no-slip conditions at the wall. The turbulent transport induced

by the advection of u_i by u_2 , as well as the turbulent pressure transport in the form of so-called pressure scrambling, is modeled in ODT by transformations affecting the scalar profiles: $u_i(t, y) \rightarrow u_i(t, f(y)) + c_i(\alpha)K(y)$. In the transformation, $u_i(t, f(y))$ is a mapping on the 1-D profile implemented at (discrete) time t . An additional modification due to a kernel function $K(y)$ and a y -uniform coefficient c_i is also applied to model the pressure-scrambling effect, see Kerstein *et al.* (2001). The coefficient c_i depends, among others, on a model parameter α which we set to a theoretical limit $\alpha = 2/3$ corresponding to equalization of u_i component available kinetic energy during mappings, see Kerstein *et al.* (2001). The mappings are sampled following a stochastic process. An (over-)sampling process in-time, which uses a sampling time-interval much smaller than the Kolmogorov time-scale of the flow, implements mappings given by a randomly sampled *eddy position* y_0 and a sampled *eddy size* l from a presumed probability density function (PDF) $h(l)$. The form of $h(l)$, however, is irrelevant. Sampled mappings are only implemented as long as the time-scale of the mapping is feasible, an *eddy turnover time* Δt_l . Feasibility is decided for the rate $(\Delta t_l)^{-1}$, following a scaling proportional to a local kinetic energy balance, see Kerstein *et al.* (2001); Klein *et al.* (2022),

$$\frac{1}{\Delta t_l} = \frac{C\nu}{l^2} \sqrt{\sum_i^3 \left(\frac{u_{i,K}l}{\nu} \right)^2} - Z \quad (4)$$

noting

$$u_{i,K} = \frac{1}{l^2} \int_l u_i(t, f(y))K(y)dy, \quad K(y) = y - f(y) \quad (5)$$

As in any turbulence model, empiricism is captured in the form of model coefficients C and Z . Mappings are only implemented for sampled *eddy events* on which Δt_l is real; that is, the quantity within the square-root in Eq. (4) must be positive. Additionally, mappings with real Δt_l must conform, on average, with a very small mean acceptance probability characterizing the (Poisson) stochastic process used for the sampling. Further details of the sampling process can be found in Lignell *et al.* (2013).

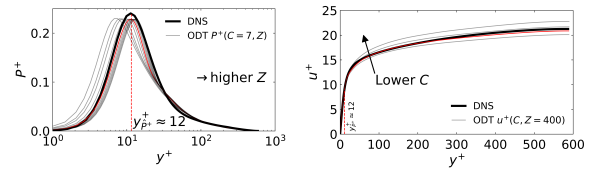


Figure 1. Effects of Z parameter variation on P^+ (left), and C parameter variation on C_f (right) in a smooth wall channel.

We comment briefly on the effect of the C and Z model parameters as observed in smooth-wall turbulent channel flows. Figure 1(left) shows the effect of Z on the turbulence kinetic energy (TKE) production P^+ (in viscous units) of a turbulent channel flow with friction Reynolds number $Re_\tau = 590$ (reference DNS data is taken from Moser *et al.* (1999)). It is notable that a change in Z causes a shift in the peak of production \hat{P}^+ , and to that extent, there is only one correct value of Z . Most notably, and as seen in Eq. (4), Z has the form of the square of a

local Reynolds number, or conversely, of a viscous coordinate. For smooth wall turbulent channel flows, \sqrt{Z} coincides with the viscous coordinate y_p^+ multiplied by the corresponding local production to dissipation ratio $\hat{P}/D_{\hat{p}}$. Based on these observations, Z is very insensitive to Re_{τ} effects. Figure 1(right) shows the effect of C on the mean streamwise velocity profile $u^+(y^+)$. There is an optimal choice of C for the best fit of the mean velocity profile, which could also correspond to the correct reproduction of the skin friction coefficient C_f predicted by DNS. Note that larger values of C cause smaller effects on C_f .

Before commenting on the obtained ODT results for rough wall flows with the described PFA suggested by Forooghi *et al.* (2018), we detail an alternative drag forcing, motivated on the basis of volume-averaging theory (VAT).

VAT-BASED DRAG PARAMETRIC FORCING

Conceptualizing the homogeneous roughness as one originated by a set of discrete roughness elements is an alternative approach which can be used to derive a drag parameterization more closely related to the surface geometry. Our starting point is to conceptualize an averaging plane of thickness Δy which will span through the entire numerical domain, see Figure 2. The thickness Δy is set as the numerical resolution of our simulation, which is capable of resolving the Kolmogorov scale of the turbulent flow. The averaging plane is a representative elementary volume (REV). The choice of the shape of the roughness elements may be arbitrary, see also Forooghi *et al.* (2017). In the current study, we work with elements in the shape of a truncated cone with a relative pre-specified base and top diameter ratio, see Figure 2.

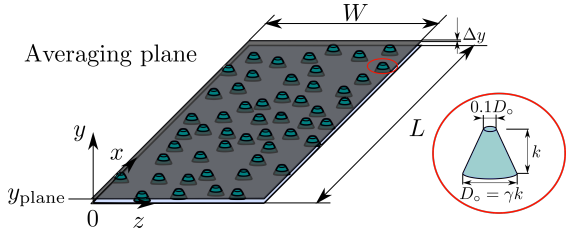


Figure 2. Averaging plane and roughness elements.

The discrete roughness elements distributed on the homogeneous rough surface yield certain statistical area moments for the surface $k(x, z)$. The first-order statistical area-moment is the melt-down height k_{MD} , that is,

$$k_{MD} = \frac{1}{LW} \int_0^L \int_0^W \tilde{k} dz dx \quad (6)$$

Here L and W are the streamwise and spanwise extent of the rough surface, respectively. The root-mean-square value k_{RMS} is the second-order moment of the deviation (with respect to the mean k_{MD}), and is calculated similarly, as well as the normalized Skewness Sk (third-order moment), see details in Forooghi *et al.* (2017). By specifying k_{MD} , k_{RMS} and Sk , it is possible to fit a PDF of the area-moments of $k(x, z)$. We choose to fit a Weibull PDF $\beta(\tilde{k}; \phi, \theta)$, with ϕ and θ as shape and scale parameters, following a strategy by Yang *et al.* (2022),

$$\beta(\tilde{k}; \phi, \theta) = \phi \theta^\phi \tilde{k}^{\phi-1} e^{-(\theta \tilde{k})^\phi} \quad (7)$$

The cumulative distribution function (CDF) associated to $\beta(\tilde{k}; \phi, \theta)$ is the porosity profile $\varepsilon(k)$, see Altland (2022). Given that only positive values can be sampled from the Weibull PDF, we use the coordinate translation $y = \tilde{k} - k_{min}$, where k_{min} is the minimum roughness height which truncates the distribution. As long as $k_{min} = 0$, the obtained PDF can be integrated analytically yielding $\varepsilon(k) = \varepsilon(y)$, that is, the wall-normal porosity profile. This assumption also implies that $\varepsilon(y=0) = 0$. For the more general case $\varepsilon(y=0) \neq 0$, which is equivalent to $\varepsilon(k_{min}) \neq 0$, as some of the cases in Forooghi *et al.* (2018), one can first calculate k_{min} for a prescribed porosity value $\varepsilon(y=0) \neq 0$ solving from the analytical CDF. That is, $k_{min} = \left\{ -\ln |1 - \varepsilon(y=0)|^{1/\phi} \right\} / \theta$. After k_{min} is obtained, we can use the transformation $\tilde{k} = y + k_{min}$, to find $\varepsilon(y)$ from the analytical CDF,

$$\varepsilon(y) = 1 - e^{-[\theta(y+k_{min})]^\phi} \quad (8)$$

In addition to $\varepsilon(y)$, we also determine wall-normal profiles for the (averaged) equivalent diameter of the discrete roughness elements $D_o(y)$ and the equivalent flow (free area) pore diameter $D_k(y)$. We stress that $D_o(y) \neq D_k(y)$. Due to the shape of the discrete roughness elements as seen in Figure 2, $D_o = \gamma k$, where γ is a constant scalar equal for all roughness elements and k is the mean roughness height. It is clear that $k \neq k_{MD}$, and in fact, k is obtained from considering the expected value of the one-point PDF of the roughness heights, i.e., a different PDF to $\beta(k; \phi, \theta)$. We can consider the roughness heights conformal with a probabilistic fractal set, as long as a sufficiently large distribution of roughness heights exists, i.e., $k_{min} \ll k_{max}$, where k_{max} is a pre-specified maximum roughness height truncating the distribution. Conceptualizing roughness as a fractal set is not a new idea, see Majumdar & Bhushan (1990). Depending on whether $k_{min} = 0$ or $k_{min} > 0$, the roughness can be characterized as a probabilistic fractal by assuming a self-similar power law distribution of heights with upper, or lower and upper truncation, respectively, see Shen (2011). In the example case of lower and upper truncation, the PDF of the stochastic roughness heights k^* is

$$\psi(k^*) = \frac{F k_{max}^{-F}}{1 - (k_{min}/k_{max})^F} (k^*)^{F-1}, \quad F > 0 \quad (9)$$

Here, F is a positive fractional exponent. This PDF has a mean value k which is the result of the converging integral $\int_{k_{min}}^{k_{max}} k^* \psi(k^*) dk^*$. The integral can be solved analytically, see Shen (2011), such that with known values of k , k_{min} and k_{max} , it is possible to estimate F . The exponent F is not necessarily the geometric fractal dimension. Rather, it is simply a fractal exponent which we take as a Korcak-law exponent, see Imre & Novotný (2016). This is done in order to estimate the total number of roughness elements in the homogeneous surface as $N_T = (k_{max}^2/k_{min}^2)^F$. Note that considering both $\beta(\tilde{k})$ and $\psi(k^*)$ is our equivalent interpretation of the need to consider both the PDF of roughness heights ($\psi(k^*)$) and their power spectrum (related to $\beta(\tilde{k})$) as in Pérez-Ràfols & Almqvist (2019) and Yang *et al.* (2022).

Considering the total base-area of the roughness, $A_b = (1 - \varepsilon(y=0))LW$, as the expected value of a distribution of roughness element diameters, i.e., $A_b = N_T(\pi/4)E[D_o^2(y=0)]$, and given the assumed shape of the roughness elements in Figure 2, we can calculate the

roughness element aspect ratio γ as

$$\gamma = \sqrt{\frac{4A_b}{\pi N_T \int_{k_{\min}}^{k_{\max}} \left\{ (k^*)^2 \psi(k^*) \right\} dk^*}} \quad (10)$$

This allows then the determination of $D_o(y)$ and $D_k(y)$ as

$$D_o(y) = \gamma k - 0.9\gamma y, \quad D_k(y) = \sqrt{\frac{4LW\varepsilon(y)}{\pi N_T}} \quad (11)$$

Since the distribution $\psi(k^*)$ allows heights $k^* > k$, but $D_o(y)$ from Eq. (11) is only valid for $y \leq k$, we superpose an exponential decay in the range $k < y \leq k_{\max}$ such that $D_o(k_{\max}) \rightarrow 0$; we take $D_o(k_{\max})$ as 1% of $D_o(y = k)$. For the next step of our model formulation, we define the volume (or surface) averaging, as well as the intrinsic averaging of the 3-D velocity field $u_i(x, y, z)$,

$$\langle u_{i,\sigma} \rangle = \frac{1}{LW} \int_0^L \int_0^W u_i \chi dz dx, \quad \langle u_{i,\sigma} \rangle^\sigma = \frac{\langle u_{i,\sigma} \rangle}{\varepsilon} \quad (12)$$

Here, χ is a unitary indicator function which is only nonzero within the fluid phase σ . To that extent, $\langle u_{i,\sigma} \rangle(y)$ and $\langle u_{i,\sigma} \rangle^\sigma(y)$ are the volume and intrinsic averaging of $u_i(x, y, z)$, respectively. All assumptions from classical VAT are considered, see Whitaker (1999). The scale separation between the roughness (horizontal) scale, i.e., the pore scale D_k , and the size of the REV is respected, such that $D_k \ll \sqrt{L \times W}$. Porosity is also considered homogeneous in the horizontal directions x and z . A decomposition of variables is performed as in Whitaker (1999), namely, $u_{i,\sigma} = \langle u_{i,\sigma} \rangle^\sigma + u''_{i,\sigma}$, noting $u_{i,\sigma} = u_i \chi$ and $p_\sigma = p \chi = \langle p \rangle^\sigma + p''_\sigma$, noting $p_\sigma = p \chi$. Double-primed variables such as p''_σ represent (non-resolved) residual quantities. Following the derivation steps in Whitaker (1999), and dropping all subindices σ , it is then possible to arrive at the volume-averaged momentum equation

$$\begin{aligned} \frac{\partial \langle u_i \rangle^\sigma}{\partial t} = & -\frac{1}{\rho} \left(\frac{p_{x=L} - p_{x=0}}{L} \right) \delta_{i1} - \frac{1}{\rho} \frac{\partial \langle p \rangle^\sigma}{\partial y} \delta_{i2} \\ & + \nu \frac{\partial^2 \langle u_i \rangle^\sigma}{\partial y^2} - \frac{1}{\varepsilon} \frac{\partial \langle u'_2 u'_i \rangle}{\partial y} + \frac{\nu}{\varepsilon} \langle u_i \rangle^\sigma \frac{\partial^2 \varepsilon}{\partial y^2} \\ & + \frac{1}{\rho \varepsilon L W} \int_{A_{\text{int}}} \left(-p'' \delta_{ij} + \mu \frac{\partial u''_i}{\partial x_j} \right) \hat{n}_j dA_{\text{int}} \end{aligned} \quad (13)$$

In the above equation, A_{int} is the interfacial area between the fluid and the roughness, δ_{ij} is 1 for $i = j$ and zero otherwise; \hat{n}_j is the normal vector in j direction of the surface with area A_{int} ; also, $(p_{x=L} - p_{x=0})/L$ is an overall streamwise pressure drop due to the homogeneous roughness. Eq. (13) was derived considering the result $\langle u_2 \rangle = 0$ from the volume-averaged continuity equation (with constant density). The fourth term on the RHS of Eq. (13) can be decomposed onto the sum of a linear (advection) part $\mathcal{M}_{\mathcal{L}}(\langle u_i \rangle)$ and a nonlinear part $\mathcal{M}_{\mathcal{N}}(\langle u_i \rangle)$. The sum of $\mathcal{M}_{\mathcal{L}}(\langle u_i \rangle)$ with the fifth and sixth terms in Eq. (13) can be modeled by means of a Darcy-Forchheimer total permeability tensor, see Whitaker (1996),

$$\begin{aligned} -\nu \varepsilon K_{T,ij}^{-1} \langle u_j \rangle^\sigma = & \frac{1}{\rho \varepsilon L W} \int_{A_{\text{int}}} \left(-p'' \delta_{ij} + \mu \frac{\partial u''_i}{\partial x_j} \right) \hat{n}_j dA_{\text{int}} \\ & - \mathcal{M}_{\mathcal{L}}(\langle u_i \rangle) + \frac{\nu}{\varepsilon} \frac{\partial^2 \varepsilon}{\partial y^2} \langle u_i \rangle^\sigma \end{aligned} \quad (14)$$

We assume an isotropic total permeability tensor equal to its streamwise component $K_{T,ij} = K_{T,xx} \delta_{ij}$. Substituting Eq. (14) on Eq. (13), and following classical VAT, we consider the asymptotic steady-state laminar flow limit neglecting the so-called Brinkman correction. In such case, the volume integration of the resulting VAT-based momentum equation leads to $\mu \varepsilon K_{T,xx}^{-1} \langle u_1 \rangle^\sigma L W \Delta y = -N_T \Delta p_o \pi \Delta y D_o$. Noting that within the REV, the presence of roughness elements is equivalent to the presence of cylindrical obstacles, we note $\Delta p_o(y)$ as the pressure drop due to one cylindrical roughness element (at wall-normal position y). $K_{T,xx}(y)$ has units m^2 , such that its corresponding dimensionless form can be obtained by division with $D_k^2(y)$, the square of the pore diameter. Denoting $\Delta p_o/L$ as dP/dx , the resulting nondimensional total permeability tensor can then be written as

$$D_k^2 K_{T,xx}^{-1} = \frac{N_T \pi D_o}{W} G, \quad G = -\frac{D_k^2}{\mu \langle u_1 \rangle} \frac{dP}{dx} \quad (15)$$

$G(y)$ is a nondimensional pressure gradient. According to this choice, we can also define a local pore Reynolds number as $\text{Re}_p(y) = \|\langle u_i \rangle\| (y) D_k(y) / \nu$. Khalifa *et al.* (2020) have obtained, for a unit-cell of a staggered array of cylinders, a quadratic regression for G , as a function of Re_p . The regression yields a very good fit for all regimes in the range $\text{Re}_p \leq \text{Re}_{p,F2}$, where $\text{Re}_{p,F2}$ is the end of the Forchheimer regime. Thus, it is possible to estimate $G(\text{Re}_p)$ using the suggested regression by Khalifa *et al.* (2020),

$$G(y) = \hat{c}_1 + \hat{c}_2 \frac{\|\langle u_i \rangle\| D_k}{\nu} + \hat{c}_3 \frac{\|\langle u_i \rangle\|^2 D_k^2}{\nu^2} \quad (16)$$

Here, \hat{c}_1 , \hat{c}_2 and \hat{c}_3 are coefficients which depend on the porosity and therefore, on the wall-normal coordinate y . Interpolation of the values of \hat{c}_1 , \hat{c}_2 and \hat{c}_3 for specific porosity values is possible. Substituting Eq. (15) and (14) on Eq. (13), while noting $(p_{x=L} - p_{x=0})/L = d\bar{p}^\sigma/dx$, we obtain the reduced modeled VAT-based momentum equation

$$\begin{aligned} \frac{\partial \langle u_i \rangle^\sigma}{\partial t} + \frac{1}{\varepsilon} \mathcal{M}_{\mathcal{N}}(\langle u_i \rangle) = & \nu \frac{\partial^2 \langle u_i \rangle^\sigma}{\partial y^2} - \nu \varepsilon \frac{N_T \pi D_o}{W} \frac{G}{D_k^2} \langle u_i \rangle^\sigma \\ & - \frac{1}{\rho} \frac{d\bar{p}^\sigma}{dx} \delta_{i1} - \frac{1}{\rho} \frac{\partial \langle p \rangle^\sigma}{\partial y} \delta_{i2} \end{aligned} \quad (17)$$

It is now easy to see, by substitution of the definition of G from Eq. (16), that we have obtained a drag parameterization which is very similar to that proposed by Forooghi *et al.* (2018). However, we now have eliminated the degrees of freedom associated to the ad-hoc parameters k_K and c_D . Figure 3 compares the forcing coefficients obtained with the VAT-based formulation with those obtained by Forooghi *et al.* (2018) for a rough surface with $k/H = 0.12$ ($k^+ = 67$, $\text{Re}_\tau \approx 500$). The coefficient associated with the linear velocity term (A -equivalent) is underestimated, while the coefficient associated with the quadratic velocity term (B -equivalent) is overestimated. The cubic velocity coefficient term from the VAT-based model is, in comparison, negligible to the other two.

We finalize the model formulation by stressing some remarks. First of all, it is noted that component $i = 2$ of Eq. (17) is simply a balance between the wall-normal pressure gradient and the nonlinear advection term $\mathcal{M}_{\mathcal{N}}(\langle u_2 \rangle)$, as in any statistically stationary and statistically streamwise homogeneous turbulent channel flow analysis. To that extent, the role of the pressure is expected to be roughly the same as that in a

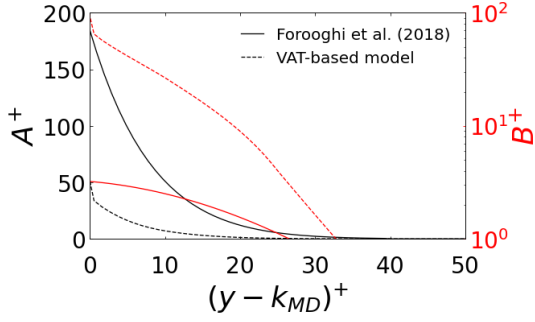


Figure 3. Drag forcing coefficient profiles, in viscous units.

classical turbulent channel, among others, responsible for re-distribution of TKE among Reynolds stress components. The role of $\mathcal{M}_{\mathcal{N}}(\langle u_i \rangle)$ is then that of a nonlinear interaction term which should be responsible for nonlinear turbulent advective TKE transport. Hence, it is easy to see the correspondence between $\mathcal{M}_{\mathcal{N}}(\langle u_i \rangle)$ and the modeled ODT turbulent advection term $\mathcal{M}(u_i)$ in Eq. (3). Note also that $\langle u_2 \rangle = 0$ by continuity, and thus, the component $i = 2$ of Eq. (17) is an over-constraint on the system. This finalizes our model formulation. Multiplying Eq. (17) by ε , and replacing the component $i = 2$ of Eq. (17) for an unconstrained model equation, the ODT governing equation for the suggested VAT-based drag forcing is

$$\frac{\partial \langle u_i \rangle}{\partial t} + \mathcal{M}(\langle u_i \rangle) = -\frac{1}{\rho} \frac{d\bar{p}}{dx} \delta_{i1} + \nu \frac{\partial^2 \langle u_i \rangle}{\partial y^2} - \nu \varepsilon \Gamma \frac{G}{D_k} \langle u_{i \neq 2} \rangle \quad (18)$$

We use $\Gamma = N_T \pi D_o / W$. We do not consider drag forcing on the $\langle u_2 \rangle$ velocity component. Also, we interpret the vector norms in Eq. (16) as the absolute value of the velocity component $\langle u_i \rangle$ for any i , as in Ferooghi *et al.* (2018).

SIMULATION RESULTS AND DISCUSSION

We carry out ODT simulations of turbulent channel flows for the surfaces with homogeneous roughness listed in Table 1. The surface with $k/H = 0.12$ is evaluated at $\text{Re}_\tau = 498$, yielding $k^+ \approx 67$. The surface with $k/H = 0.19$ is evaluated at $\text{Re}_\tau = 499$ yielding $k^+ \approx 110$. It is noted that the surface with $k/H = 0.19$ does not have a height distribution. Thus, it cannot be characterized by a fractal set. For this surface, we provide $N_T = 1080$ in order to estimate γ .

Table 1. Characterization of the evaluated homogeneous rough surfaces. Note that $\varepsilon(0)$ refers to $\varepsilon(y = 0)$.

k/H	k_{MD}/H	k_{RMS}/H	Sk	k_{max}/H	$\varepsilon(0)$
0.12	0.074	0.045	0.21	0.21	0.045
0.19	0.1	0.045	0.21	0.19	0

We define $\text{Re}_\tau = u_\tau(H - k_{MD})/\nu$, where H is the half-height of the computational channel. With this definition, k_{MD} acts as a virtual origin. Below this origin, the forcing enforces artificial no-slip conditions on the u_1 and u_3 velocity components. In any case, the traditional no-slip boundary conditions at $y = 0$ and $y = 2H$ are respected. First, ODT simulations are carried out using both the forcing specified by Ferooghi *et al.* (2018), e.g., for case $k/H = 0.12$ using the coefficients

shown in Figure 3 (parameters $k_K = 25$ and $c_D = 1.5$ in Eq. (2)). Next, the alternative VAT-based forcing is used. The prescribed ODT model Z for these simulations is estimated as in smooth channels, but considering the position of the viscous coordinate y_β^+ being approximated by k_{max}^+ , usually close, see Yuan & Piomelli (2014). To that extent, the relevant coordinate, measured from the virtual origin, is $k_{max}^+ - k_{MD}^+$. This yields $Z = 5350$ for the fractal roughness case and $Z = 2500$ for the non-fractal case. The values of the C parameter are calibrated for best matching of the mean velocity profile or of C_f . We find $C = 3$ when using the forcing from Ferooghi *et al.* (2018) and $C = 4$ when using the VAT-based forcing for the fractal roughness case. For both types of forcing, we find $C = 2.5$ for the non-fractal roughness.

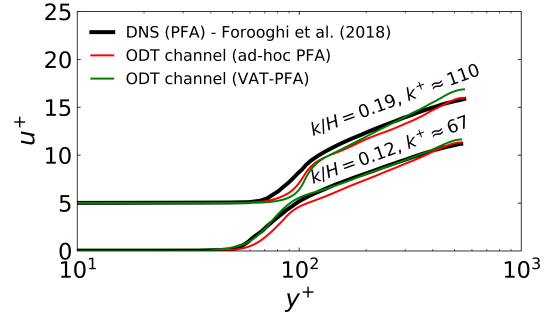


Figure 4. Mean velocity profiles. Case $k/H = 0.19$ is shifted upwards 5 viscous units for better visualization.

Figure 4 shows a comparison of the wall-normal mean streamwise velocity profiles. Reasonable reproduction of the mean velocity profile is obtained in all cases. Arguably, the simulation of the non-fractal roughness surface yields worse results when compared to the fractal roughness case. The reproduction of the mean velocity profile in the fractal roughness case using the VAT-based forcing is remarkable. Figure 5 shows the contributions to the stress balance affecting u_1 obtained when using the ad-hoc forcing from Ferooghi *et al.* (2018) in ODT. The value of the wall-shear stress is computed using the methodology in Ferooghi *et al.* (2017), i.e., linearly extrapolating the value of the total stress to the virtual origin k_{MD} . Besides the reasonable reproduction of the Reynolds stress in comparison to the DNS data of Ferooghi *et al.* (2018), we find that the position y_β^+ coincides exactly with the coordinate k_{max}^+ . Despite both coordinates being close to each other, this need not be the case, as discussed in Yuan & Piomelli (2014). The viscous stress also shows a very steep decrease immediately after k_{max}^+ . Figure 6 shows the same stress contributions, but now using the suggested VAT-based forcing. Less steep gradients are observed for the viscous stress. Also remarkable is the fact that $y_\beta^+ \neq k_{max}^+$, a more physical result.

CONCLUSION

We presented an overview of the application of the ODT model for turbulent channel flows with homogeneous roughness. To that extent, a PFA for the roughness-induced drag was used in ODT. We have verified the effects of using the proposed PFA in Ferooghi *et al.* (2018). Although model results using this forcing are reasonable, there is an inherent limitation in the suggested PFA in the sense that it introduces two arbitrary coefficients, k_K and c_D , which cannot be derived from

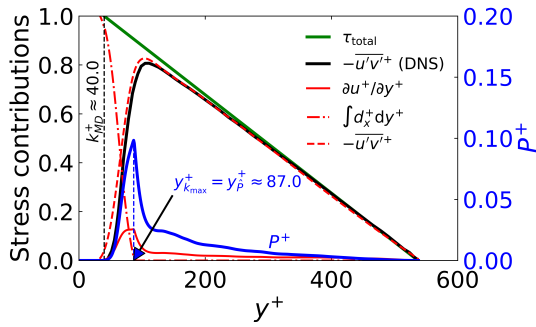


Figure 5. Stress contributions using drag PFA from Forooghi *et al.* (2018) in ODT.

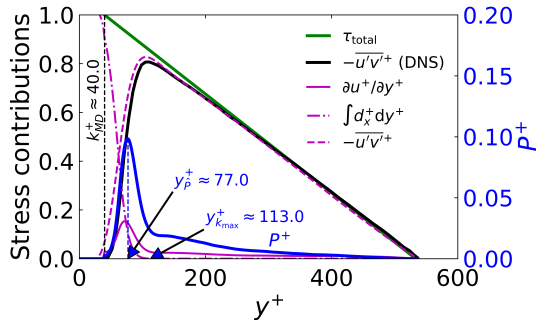


Figure 6. Same as Fig. 5 but using VAT-based drag PFA.

first principles. These were obtained in Forooghi *et al.* (2018) by a DNS calibration procedure. This is unjustifiably expensive from the computational point of view. To address this issue, we have suggested an alternative on the basis of VAT. By doing so, we have also identified correspondences with nondimensional drag representations for staggered cylinder arrays in Khalifa *et al.* (2020). The alternative VAT-based forcing has no arbitrary coefficients on its formulation. Nonetheless, as a turbulence model, ODT is not exempt from empiricism, and also introduces additional model parameters. We argue that for the case at discussion, there is only one model parameter which needs to be calibrated in ODT, the C parameter. This is still an improvement from the previous DNS PFA with two different model coefficients. We also verified that the suggested VAT-based forcing is able to deliver more physical-based results in ODT, at least concerning the stress contributions and TKE production. Thus, this study advances the State of the Art by providing a parametric drag representation which is directly obtainable from the geometric characterization of the roughness. Higher order flow statistical moments, which can also be obtained without further alteration of the ODT model formulation, will be addressed in future work.

REFERENCES

Altland, S. 2022 A Distributed Element Roughness Model Based on the Double Averaged Navier-Stokes Equations. PhD thesis.

Busse, A., Lütznert, M. & Sandham, N. D. 2015 Direct numerical simulation of turbulent flow over a rough surface based on a surface scan. *Comput. Fluids* **116**, 129–147.

Busse, A. & Sandham, N. D. 2012 Parametric forcing approach to rough-wall turbulent channel flow. *J. Fluid Mech.* **712**, 169–202.

Chung, D., Hutchins, N., Schultz, M. P. & Flack, K. A. 2021

Predicting the drag of rough surfaces. *Annu. Rev. Fluid Mech.* **53**, 439–471.

Cooke, J., Jerolmack, D. & Park, G. I. 2024 Mesoscale structure of the atmospheric boundary layer across a natural roughness transition. *PNAS* **121** (13), e2320216121.

Forooghi, P., Frohnapfel, B., Magagnato, F. & Busse, A. 2018 A modified Parametric Forcing Approach for modelling of roughness. *Int. J. Heat Fluid Flow* **71**, 200–209.

Forooghi, P., Stroh, A., Magagnato, F., Jakirlić, S. & Frohnapfel, B. 2017 Toward a Universal Roughness Correlation. *J. Fluids Eng.* **139** (12).

Imre, A. R. & Novotný, J. 2016 Fractals and the Korcak-law: a history and a correction. *Eur. Phys. J. H* **41** (1), 69–91.

Kerstein, A. R. 1999 One-dimensional turbulence: model formulation and application to homogeneous turbulence, shear flows, and buoyant stratified flows. *J. Fluid Mech.* **392**, 277–334.

Kerstein, A. R., Ashurst, W. T., Wunsch, S. & Nilsen, V. 2001 One-dimensional turbulence: Vector formulation and application to free-shear flows. *J. Fluid Mech.* **447**, 85–109.

Khalifa, Z., Pocher, L. & Tilton, N. 2020 Regimes of flow through cylinder arrays subject to steady pressure gradients. *Int. J. Heat Mass Transfer* **159**, 120072.

Klein, M., Schmidt, H. & Lignell, D. O. 2022 Stochastic modeling of surface scalar-flux fluctuations in turbulent channel flow using one-dimensional turbulence. *Int. J. Heat Fluid Flow* **93**, 108889.

Lignell, D., Kerstein, A. R., Sun, G. & Monson, E. 2013 Mesh adaption for efficient multiscale implementation of One-Dimensional Turbulence. *Theor. Comput. Fluid Dyn.* **27** (3-4), 273–295.

Majumdar, A. & Bhushan, B. 1990 Role of Fractal Geometry in Roughness Characterization and Contact Mechanics of Surfaces. *J. Tribol.* **112** (2), 205–216.

Moser, R., Kim, J. & Mansour, N. 1999 Direct Numerical Simulation of turbulent channel flow up to $Re_t = 590$. *Phys. Fluids* **11** (4), 943–945.

Pérez-Ràfols, F. & Almqvist, A. 2019 Generating randomly rough surfaces with given height probability distribution and power spectrum. *Tribol. Int.* **131**, 591–604.

Shen, W. 2011 Fractal invariable distribution and its application in large-sized and super large-sized mineral deposits. *Geoscience Frontiers* **2** (1), 87–91.

Thorat, U., Jones, M., Woollam, R., Owen, J., Barker, R., Thompson, H. & de Boer, G. 2024 Computational fluid dynamics driven mass transfer model for the prediction of CO₂ corrosion in pipelines. *J. Pipeline Sci. Eng.* **4** (1), 100148.

Toja-Silva, F., Kono, T., Peralta, C., Lopez-Garcia, O. & Chen, J. 2018 A review of computational fluid dynamics (CFD) simulations of the wind flow around buildings for urban wind energy exploitation. *J. Wind Eng. Ind. Aerodyn.* **180**, 66–87.

Whitaker, S. 1996 The Forchheimer equation: A theoretical development. *Transp. Porous Med.* **25**, 27–61.

Whitaker, S. 1999 *The Method of Volume Averaging*, vol. 13. Springer Science & Business Media.

Yang, J., Stroh, A., Chung, D. & Forooghi, P. 2022 Direct numerical simulation-based characterization of pseudo-random roughness in minimal channels. *J. Fluid Mech.* **941**, A47.

Yuan, J. & Piomelli, U. 2014 Roughness effects on the Reynolds stress budgets in near-wall turbulence. *J. Fluid Mech.* **760**, R1.